ACS OMEGA

http://pubs.acs.org/journal/acsodf

Article

Morphological Features of Fractures Developed by Direct Shearing of Intact Granites after Water Cooling Cycles

Haiyang Jiang, Tao Chen,* Fengxin Kang, Fugang Wang, Liangliang Guo, and Yanling Cao

Cite This: *ACS Omega* 2023, 8, 13639−13648

Read Online

ACCESS | Metrics & More | Article Recommendations

ABSTRACT: Rock fractures are considered as favorable objects for enhanced geothermal development. The fracture morphologies play an important role in enhanced geothermal development. Therefore, the study of fracture morphologies has a certain guiding significance for the geothermal reservoir. Water cooling and water cooling cycles can change the morphology of fracture surfaces formed by the shear failure of intact granites. To date, however, there is little work on the effect of water cooling and water cooling cycles on the morphology of fracture surfaces formed by direct shearing of intact granites. In this study, the direct shear tests of intact granites treated by water cooling cycles at different temperatures were conducted, and the variations in the laws of shear strength of intact granites and morphologies of fracture surfaces with temperature or cycle times were analyzed. Test results showed that the shear strength and shear stiffness of intact granites decreased nonlinearly with the increase of temperature or cycle times, but the height and apparent dip angle of asperities on the fracture surface increased with the increase of temperature or cycle times, and the overall uniformity of the fracture surface was improved. The height distribution frequency of asperities on fracture surfaces can be divided into four types: right-biased peak type, left-biased peak type, left-biased middle peak, and left-biased flat peak. The asperities on the fracture surface formed by the shearing of intact granites have asymmetric characteristics. The maximum apparent dip angle and average apparent dip angle in the reverse shear direction are larger than those in the shear direction, and the initial contact area ratio between the shear direction and reverse shear direction is in the range of fluctuation between 1.4 and 2.

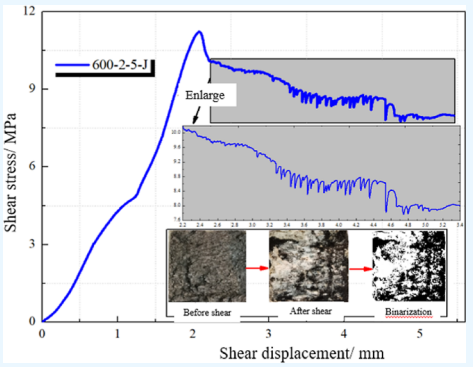

1. INTRODUCTION

Power transmission and heating supply are an important part of the building construction process, so the development and utilization of clean energy are of great significance to building construction. An enhanced geothermal system (EGS) has the advantages of abundant reserves, wide distribution, and recycling, so it is considered by many countries in the world as the most potential clean energy to replace coal, oil, and other fossil fuels in the future.[1,2] However, due to a lack of comprehensive understanding of EGSs, there are still many issues in the process of geothermal energy mining, such as low heat recovery rate, serious leakage, induced earthquakes, and so forth. Therefore, the research on the related problems of EGS is of great significance for promoting the development of geothermal energy and the adjustment of energy structure.

The existence of a large number of isolated fractures is a major feature of geothermal reservoir structures. Connecting fractures to form a highly permeable fracture network channel is a prerequisite for the efficient exploitation of geothermal energy. Water injection fracturing[3−5] is considered to be an effective method to connect fractures. However, in the process of water injection fracturing, cold water injection is bound to cause a quenching impact on the rock; in the long-term fracturing process, the quenching impact on high-temperature rock occurs repeatedly, which causes irrecoverable damage to the rock. To date, scholars have carried out a large number of indoor-scale experimental studies on the effects of water cooling and water cooling cycles on the physical and mechanical properties of rock. Kumari et al.[6] revealed that water quenching can increase the permeability of granites. Shen et al.[7] proved that water quenching can reduce wave velocity and apparent resistivity. Kim et al.[8] proposed that water quenching can increase thermal damage on the surface of granites but has a negligible effect on the interior of granite. Isaka et al.[9] found that the water quenching promoted the interconnection of granite fractures. Fan et al.[10] indicated that the spatial gradient distribution of water quenching-induced damage increased as the preheating temperature increased and then decreased significantly above 600 °C. Wu et al.[11] compared the effects of water cooling and air cooling on the tensile strength of granite and revealed that

Received: November 29, 2022
Accepted: March 21, 2023
Published: April 3, 2023

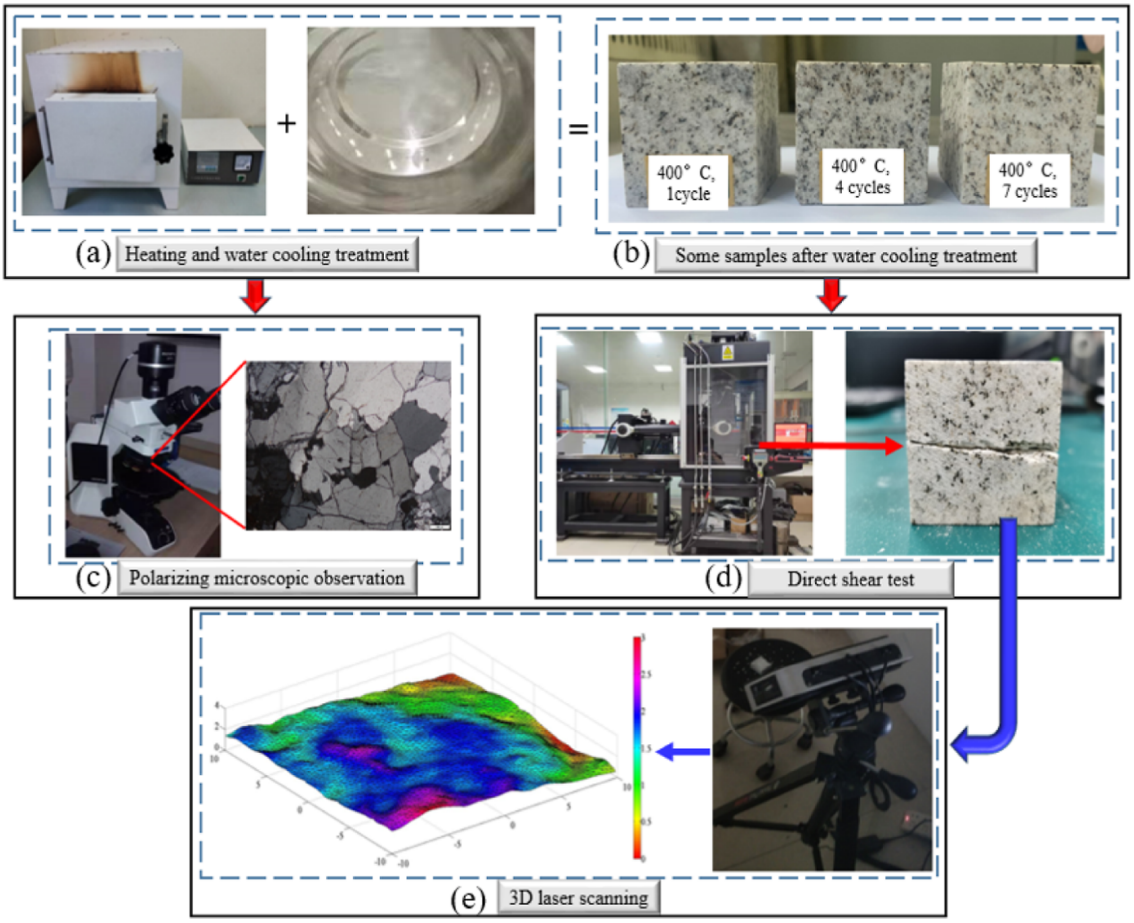

Figure 1. Test equipment.

granite damage was similar regardless of the cooling methods at temperatures less than 400 °C. Zhu et al.[12] thought that uniaxial compressive strength and tensile strength decreased obviously with increasing water cooling cycles. Hu et al.[13] found that the increase in the number of quenching cycles reduced the heat transfer capacity of the granite. Junique et al.[14] concluded that the porosity, water uptake, size, and volume of cracks increased, while P wave velocity, S wave velocity, and Young's modulus decreased with the increase of quenching cycles. Xu and Sun[15] investigated the effects of quenching cycles on the tensile strength of granites and determined that the static tensile strength decreased with increasing temperature and quenching cycles.

After the failure of the rock, a fracture surface with a certain morphology will be formed. Fractures affected by high stress are in a closed state. Therefore, it is necessary to continue injecting high-pressure water to promote the dilatancy and sliding of closed fractures to improve the aperture of fractures. This process is called hydraulic shearing,[16−18] which is a very key step in the process of enhancing the permeability in EGSs. The morphology of the fracture surface is the main factor affecting the selection of hydraulic parameters, and it is significantly affected by geological factors. Therefore, a large number of scholars have studied the morphological characteristics of fracture surfaces formed under different influencing factors. Khosravi et al.[19] found that the sample shape and loading direction both have an important influence on the fracture roughness induced by Brazilian testing. Seredin et al.[20] investigated the influence of failure modes on morphologies by conducting splitting, uniaxial, and triaxial compression tests. Liu et al.[21] indicated that the increase in confining pressure can reduce the roughness of fracture surfaces developed by direct tension, but the increase in loading rate increases the roughness of fracture surfaces. Chen et al.[22] drew a conclusion that water−rock interaction can increase the height contour, height discreteness, and deviation of fracture surfaces formed by the direct shearing test. Yang et al.[23] studied the effect of normal stress on morphologies of fracture surfaces developed by direct shearing of intact red sandstone. Water cooling and water cooling cycles are common phenomena in the development of EGSs, and they can change the morphology of fracture surfaces. To date, however, there is little work on the effect of water cooling and water cooling cycles on the morphology of fracture surfaces formed by direct shearing of intact granites.

This study aims to quantitatively characterize the morphology of fracture surfaces developed by direct shearing of intact granites treated by water cooling cycles at different temperatures. The research work was mainly carried out in the following parts: first, granites were treated by different water cooling cycles at different temperatures. Second, the shear strengths of granites treated by different water cooling cycles at different temperatures were obtained, with asperities as the main component of fractures, and the variations in the laws of asperities in the fracture surfaces with different water cooling cycles at different temperatures were described quantitatively. Last, the influence mechanism of temperature and cycle times on the morphology of fractures was analyzed from the mesoscopic point of view.

https://doi.org/10.1021/acsomega.2c07600
ACS Omega 2023, 8, 13639−13648

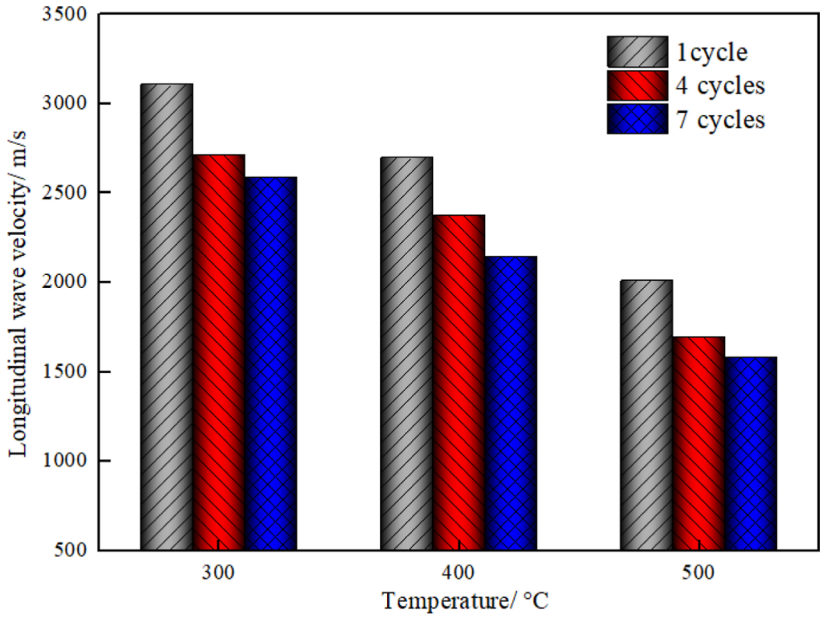

Figure 2. Longitudinal wave velocity of granites treated with different water cooling cycles.

2. SPECIMEN MATERIALS AND TEST METHODS

2.1. Specimen Materials. The granite in this test was taken from Weihai, Shandong Province, China. The granite sample had an average density of 2.69 g/cm^3 and an initial porosity of 0.49%. Using the International Society for Rock Mechanics and Rock Engineering (ISRM)'s suggested method (ref 24), the granite was processed into a cube of 50 mm × 50 mm × 50 mm.

2.2. Test Methods. *2.2.1. Heating and Cooling Scheme of Granites.* Experts in the geothermal field believe that an EGS has better research value only when the temperature is greater than or equal to 300 °C.[25,26] Therefore, we set three temperature levels of 300, 400, and 500 °C as the research object in this paper.

First, the granites were divided into three groups based on the target temperatures (300, 400, and 500 °C). The granites treated by different water cycles in each group were numbered; for example, for a heating temperature of 300 °C and one water cycle, the sample was numbered 300-1.

Second, to avoid thermal cracking during heating, each group of granites was heated to the target temperature at a slow heating rate of 5 °C/min.[27,28] Simultaneously, to ensure uniform heating of granites, the target temperature was held constant for 6 h in a furnace. Subsequently, granites were quickly placed into a prepared container containing normal-temperature water until granites were cooled to the normal temperature, as shown in Figure 1a; this process was denoted as a water cooling cycle. In the process of water cooling, water can enter the granite through the cracks formed by the heating process. Therefore, to eliminate the influence of water in the cracks on the experimental results, granites need to be placed into a drying oven for 24 h before the next cycle. The above steps were repetitively operated to complete four cycles and seven cycles of water cooling treatment on granites.

2.2.2. Direct Shear Test. The direct shear tests were conducted by using the MTS 816.01 equipment, as shown in Figure 1d. The detailed test steps were as follows.

(1) An axial load was applied up to 20 MPa at a loading rate of 0.2 MPa/s, and subsequently, the target value was kept unchanged.

(2) The force-controlled loading mode was adopted in the shear direction; the loading rate was 0.1 MPa/s until the failure of intact granites.

2.3. 3D Laser Scanning Test and Point Cloud Data Processing. After the shear failure of granites, a 3D-ML-130 nonpoint contact laser scanning system was used to obtain fracture surfaces developed by direct shearing treated by different water cooling conditions, as shown in Figure 1e. The scanning rate was 220,000 times/s, the measurement accuracy was 0.02 mm, and the range of a single measurement was 220 mm × 180 mm. To accurately obtain the 3D morphological features of fracture surfaces, a 0.3 mm sampling interval was employed in the scanning.[29]

Subsequently, the point cloud data were imported into Geomagic Studio software, packaged into surfaces, and preprocessed for noise reduction and hole filling. Subsequently, the packaging surfaces were discretized into points and imported into MATLAB calculation software. Finally, the point cloud data were discretized and constructed using the Delaunay triangulation algorithm.

3. RESULTS AND DISCUSSION

3.1. Longitudinal Wave Velocity. Longitudinal wave velocity is an important index for reflecting the integrity and compactness of rock. As shown in Figure 2, we can find that the longitudinal wave velocity of granite decreases significantly with the increase of temperature or the number of cycles. These results show that the increase of both temperature and cycle times can aggravate the generation of new fractures in the rock matrix and the development of primary fractures, resulting in a significant decrease in longitudinal wave velocity.

3.2. Peak Shear Strength and Shear Stiffness. Figure 3 shows the shear stress−shear displacement curves of intact granites treated with water cooling at different temperatures. All curves have similar variation trends with the shear displacement, and they mainly include the linear growth stage and nonlinear growth stage.

Figure 4a shows the variation in the peak shear strength of intact granites treated with water cooling at different temper-

https://doi.org/10.1021/acsomega.2c07600
ACS Omega 2023, 8, 13639−13648

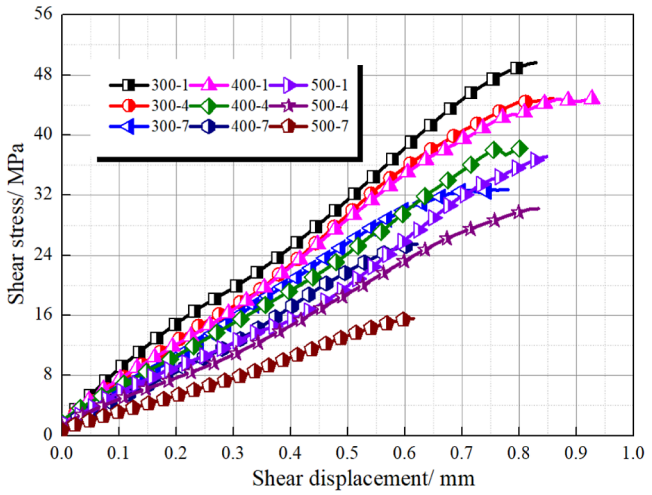

Figure 3. Shear stress−shear displacement curves.

atures. The peak shear strength of granites treated with water cooling at different temperatures has a similar variation law with the increase of cycle times, and they all showed a nonlinear decreasing law.

The peak shear strength of granite is nonlinear with the number of cycles, as shown in Figure 4a. When the temperature is 300 °C, as the number of water cooling cycles increases from one to seven, the peak shear strength decreases from 49.65 to 32.73 MPa, with a decreasing amplitude of 34.1%. When the temperature is 400 °C, as the number of water cooling cycles increases from one to seven, the peak shear strength decreases from 44.84 to 25.50 MPa, decreasing by 47.8%. When the temperature is 500 °C, as the number of water cooling cycles increases from one to seven, the peak shear strength decreases from 37.07 to 15.56 MPa, decreasing by 58.1%. The number of cycles can promote the decrease of the shear strength of granites; the higher the temperature, the greater the decrease in amplitude of shear strength with the number of cycles.

In addition, the shear stiffness has a similar change trend with the number of cycles: the higher the temperature, the greater the decrease in the amplitude of shear stiffness with the number of cycles, as shown in Figure 4b.

3.3. 3D Morphological Features. After water cooling at different temperatures and different cycle times, granites produce fractures with different morphological characteristics by the direct shear test, as shown in Figure 5a. Asperity is the main component of fracture surfaces, and its structural characteristics determine the mechanical behavior of fracture surfaces.

Asperity is the main component of fractures, and its structure basically determines the morphology of fractures. The height and apparent dip angle are two important parameters to describe the asperity features. Therefore, in order to quantitatively describe the morphological characteristics of the fracture surface developed by direct shearing of granites treated with water cooling at different temperatures, the height and apparent dip angle distribution were analyzed.

3.3.1. Height of Asperities on the Fracture Surface. The height of asperities on fracture surfaces can be obtained from eq 1.

$$H_i = N_i - \min(N_1, N_2, N_3, \cdots N_{n-1}, N_n) \quad (1)$$

where N_i is the absolute height of asperities and H_i is the relative height value of asperities.

The mean height of asperities on fracture surfaces can be obtained from eq 2.

$$\mu = \frac{1}{n}\sum_{i=1}^{n} H_i \quad (2)$$

The variance of height distribution of asperities on the fracture surface can be obtained by eq 3.

$$\sigma^2 = \frac{1}{n}\sum_{n=i}^{n} (H_i - \bar{H})^2 \quad (3)$$

Skew (H) is the skewness of the height distribution of asperities; it can be used to describe the asymmetric height distribution of asperities on fracture surfaces. The skewness can be obtained by eq 4.

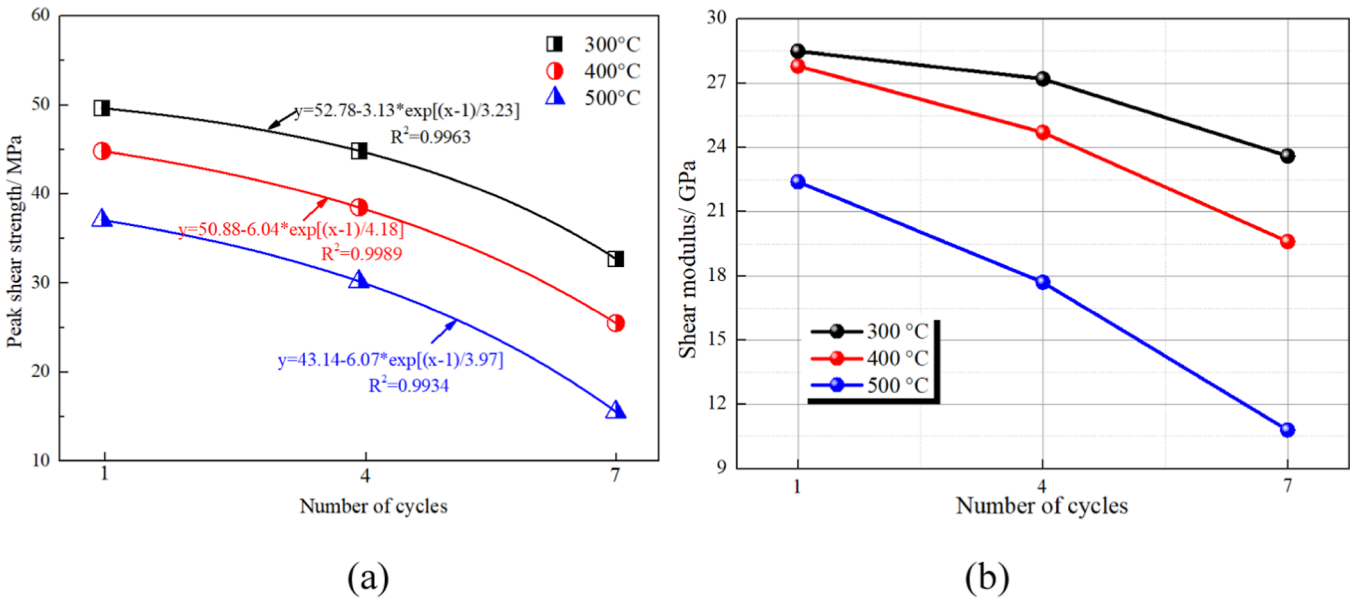

Figure 4. (a) Peak shear strength and (b) shear stiffness treated with water cooling at different temperatures.

https://doi.org/10.1021/acsomega.2c07600
ACS Omega 2023, 8, 13639−13648

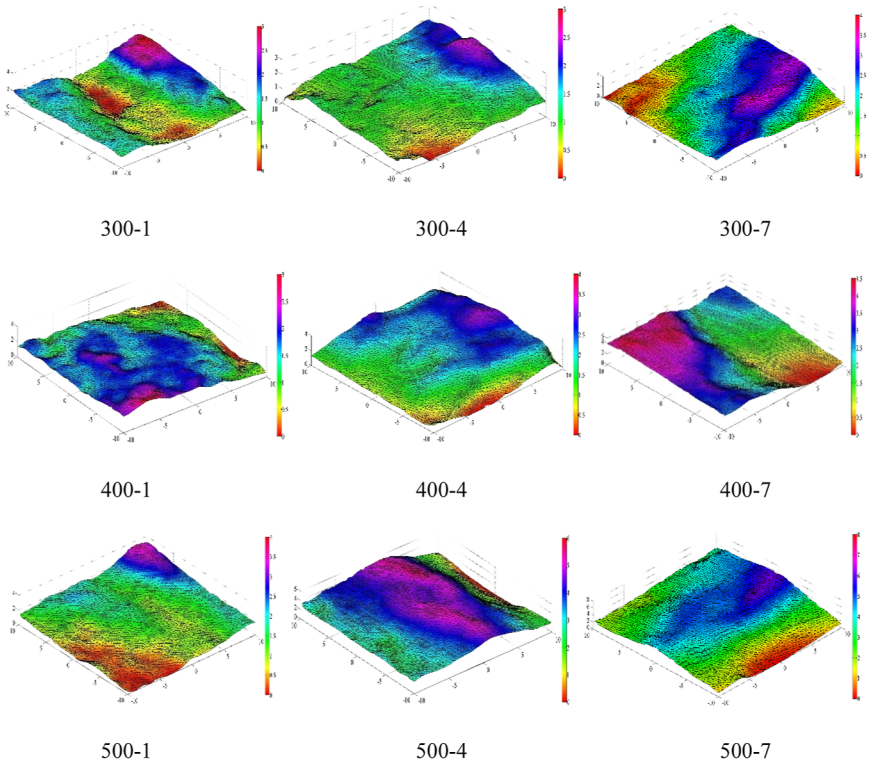

(a) 3D morphological cloud image

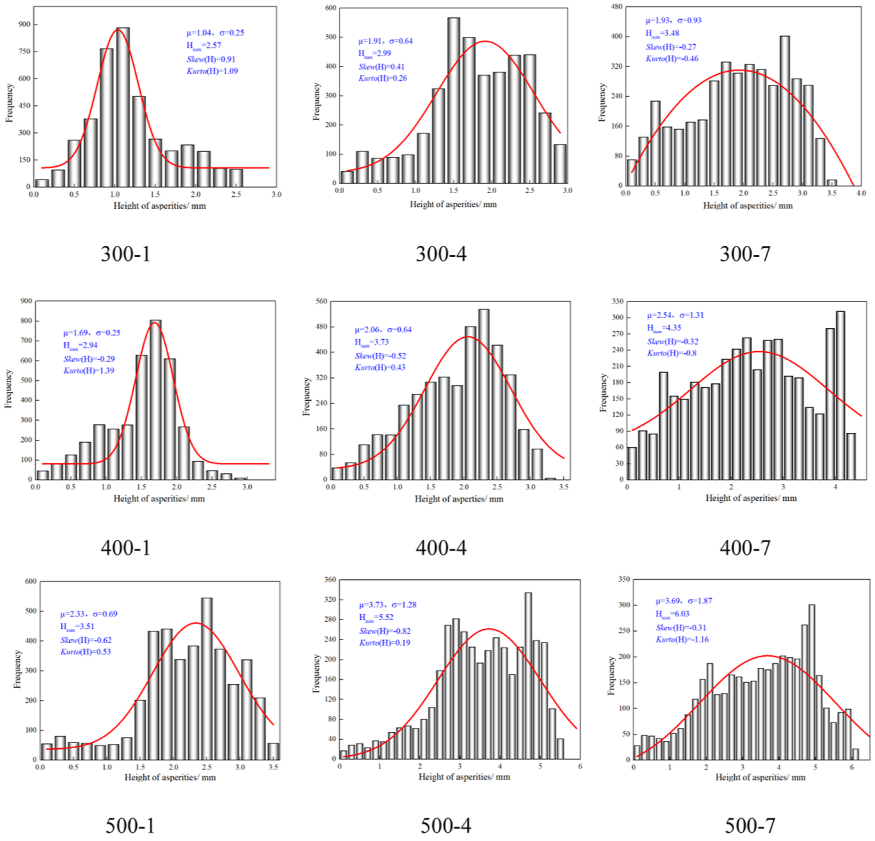

(b) Height distribution of asperities

Figure 5. 3D morphology and height distribution of asperities on fracture surfaces.

https://doi.org/10.1021/acsomega.2c07600
ACS Omega 2023, 8, 13639−13648

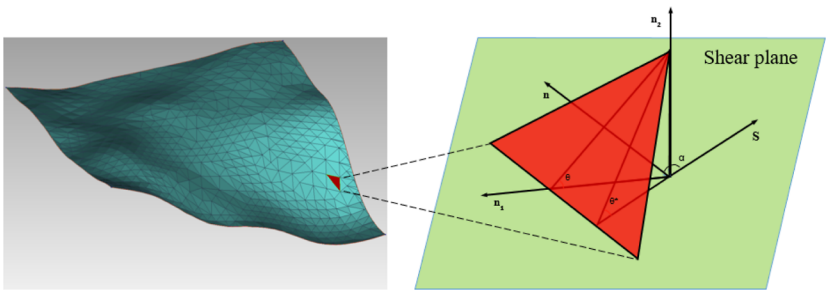

Figure 6. Geometrical identification of the apparent dip angle.

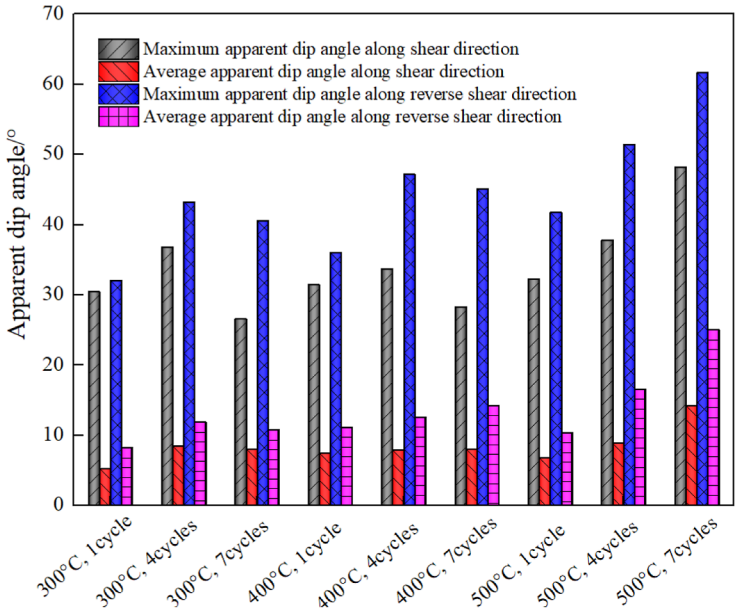

(a) The apparent dip angle of shear direction and reverse shear direction

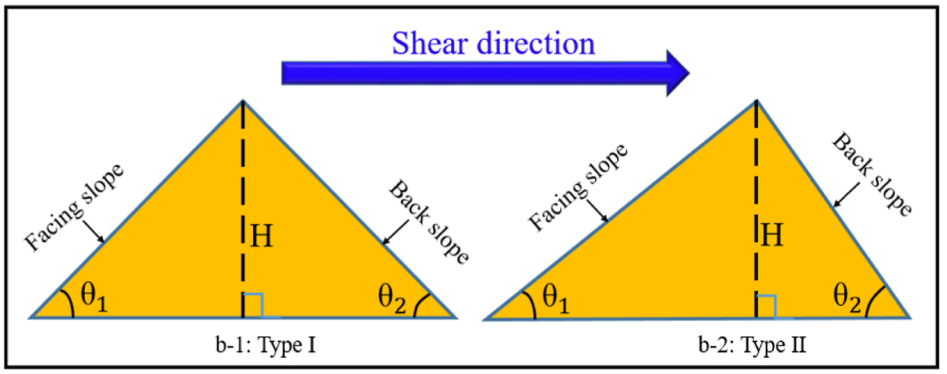

(b) Asperities structure

Figure 7. Apparent dip angle and asperities' structure in the shear direction and reverse shear direction.

$$\text{Skew}\ (H) = \frac{1}{n}\sum_{i=1}^{n}\left(\left(\frac{H_i - \bar{H}}{\sigma}\right)^3\right) \quad (4)$$

$$\text{Kurto}\ (H) = \frac{1}{n}\sum_{i=1}^{n}\left(\left(\frac{H_i - \bar{H}}{\sigma}\right)^4\right) - 3 \quad (5)$$

Kurto (H) is the kurtosis of height distribution of asperities; it can be used to describe the uniformity of height distribution of asperities. Kurtosis can be obtained by eq 5.

Figure 5b displays the height frequency histogram distributions of asperities, and they all show an approximately normal distribution. The height distribution frequency of asperities on fracture surfaces treated under different conditions can be divided into four types: right-biased peak type, left-biased peak type, left-biased middle peak, and left-biased flat peak.

https://doi.org/10.1021/acsomega.2c07600
ACS Omega 2023, 8, 13639−13648

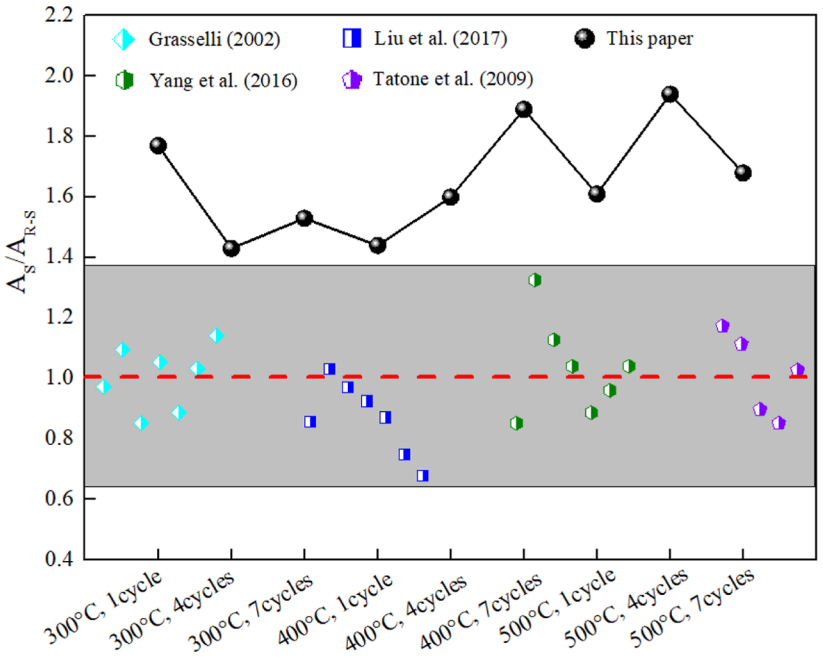

Figure 8. Initial area ratio of the shear direction to reverse shear direction.

After one water cooling cycle treatment, as the temperature increases from 300 to 500 °C, the distribution of asperities' height changes from the right-biased peak type to the left-biased peak type and then to the left-biased middle peak; the skewness value changes from positive to negative. This phenomenon indicates that the number of asperities above the average height value is more than the number of asperities below the average height value (the lower height of asperities was lower than the average height of asperities, and the higher height of asperities was higher than the average height of asperities). The maximum height of asperities increased from 2.57 to 3.51 mm, that is, an increase of 36.6%, and the mean height of asperities increased from 1.04 to 2.33 mm, that is, an increase of 124.0%. In addition, we found that kurtosis decreases with the increase in temperature, which indicates that the increase in temperature can not only increase the height of asperities but also can improve the overall uniformity of asperities' height distribution on fracture surfaces. The height distribution of asperities on fracture surfaces was affected obviously by the temperature.

The number of cycles is also an important factor affecting the morphology of fracture surfaces. At 300 °C, with the increase of cycles, the distribution of asperities' height changes from the right-biased peak type to the left-biased middle peak and then to the left-biased flat peak. When the temperature is 400 °C, the distribution of asperities' height changes from the left-biased peak type to the left-biased flat peak. Under the conditions of 500 °C, the variation of height distribution of asperities changes from the left-biased middle peak to the left-biased flat peak. The number of cycles increased the overall height of asperities and uniformity of fracture surfaces.

3.3.2. Apparent Dip Angle of Asperities on the Fracture Surface. The apparent dip angle is an important parameter for describing the 3D roughness of fracture surfaces. Figure 6 shows the 3D spatial position of the apparent dip angle; the apparent dip can be obtained by using eqs 6−8.

$$\theta = \cos^{-1}\left(\frac{n\cdot n_2}{|n|\cdot|n_2|}\right) \tag{6}$$

$$\alpha = \cos^{-1}\left(\frac{s\cdot n_1}{|s|\cdot|n_1|}\right) \tag{7}$$

$$\theta^* = \tan^{-1}(-\tan(\theta)\cdot\cos(\alpha)) \tag{8}$$

where α is the angle between n_1 and s, θ is the angle between the triangle and the sliding plane, θ^* is the apparent dip angle of the triangular element, s is the sliding vector of the failure surface, n_2 is the outer normal vector of the sliding plane, n is the outer normal vector of the triangle, and n_1 is the projection vector of n on the sliding plane.

Figure 7a shows the variation of the maximum apparent dip angle and average apparent dip angle of the shear direction and reverse shear direction treated at different temperatures and different cycle times. The maximum apparent dip angle and average apparent dip angle of the shear direction and reverse shear direction increase as a whole with temperature and cycle times.

After being treated at different temperatures and cycle times, the maximum apparent dip angle of asperities on the fracture surface along the shear direction is in the range of 30−49°; the average apparent dip angle is in the range of 5−15°, the maximum apparent dip angle of asperities along the reverse shear direction is in the range of 32−62°, and the average apparent dip angle is in the range of 8−26°; these results show that the asperity structures developed by direct shearing treated at different temperatures and cycle times have typical asymmetric characteristics. In addition, it is worth noting that the maximum apparent dip angle and average apparent dip angle of the reverse shear direction are generally larger than those in the shear direction, and the result is different from previous studies: previous studies commonly indicated that the asperities' structure is symmetrical, and the asperity structure is shown in Figure 7b-1; however, the asperity structure developed by direct shearing treated by water cooling at different temperatures has obvious asymmetry, and the asperities tend to exist in the form of Figure 7b-2 ($\theta_1 < \theta_2$).

https://doi.org/10.1021/acsomega.2c07600
ACS Omega 2023, 8, 13639−13648

In order to confirm that the conceptual model of the asperity structure proposed by us is suitable for describing the fracture surface developed and treated at different temperatures and cycle times, the initial area ratio of the shear direction to reverse the shear direction of asperities was further analyzed, as shown in eq 9.

$$\delta = A_S/A_{R\text{-}S} \tag{9}$$

where A_S is the initial contact area in the shear direction and $A_{R\text{-}S}$ is the initial contact area in the reverse shear direction.

By analyzing the data of previous studies,[30−32] we found that the initial contact area ratio between the shear direction and reverse shear direction fluctuated around 0.6, as shown in Figure 8. However, the initial contact area ratio between the shear direction and reverse shear direction obtained in this paper is generally greater than 1.4, and the maximum value is close to 2. The test results proved that the asperity structure of the fracture surface in this paper is indeed different from that in the previous research; the conceptual model of the asperity structure proposed by us is correct, and it is suitable for characterizing the asperity structure on the fracture surface treated with water cooling cycles at different temperatures.

3.4. 3D Roughness of Fracture Surfaces. Liu et al.[33−35] confirmed that $A_0\theta_{max}{}^*/(C + 1)$ can well describe the 3D roughness of fracture surfaces. It can be found from Figure 9 that

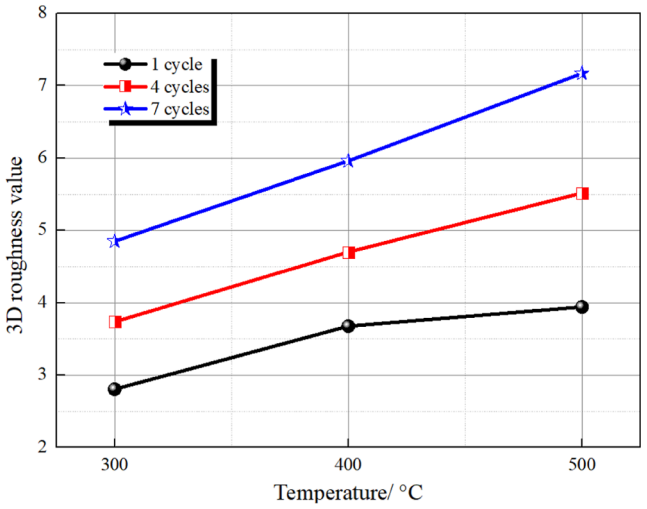

Figure 9. 3D roughness value of fracture surface.

the roughness of fracture surfaces increases with the increase of temperature under the conditions of cycle times being constant. When the number of cycles is 1, 4, and 7, respectively, as the temperature increases from 300 to 500 °C, the roughness of the fracture surface increases by 1.14, 1.78, and 2.32, respectively, with an increase of 40.7, 47.6, and 62.2%, respectively. When the temperature is kept constant at 300, 400, and 500 °C, respectively, the roughness of the fracture surface increases by 2.05, 2.29, and 3.22, respectively, with the increase of cycle times from 1 to 7. The temperature and cycle times both increase the 3D roughness of the fracture surface.

3.5. Influence Mechanism of Temperature and Number of Cycles on Fracture Morphology. Based on the above research, it is known that not only the shear strength of intact granites treated at high temperatures and water cooling cycles is reduced but also the morphology of the fracture surface formed by direct shearing changes greatly. In fact, the macroscopic fracturing features of granites are caused by numerous small fractures and defect development and connection on the mesoscale. In order to further reveal the main cause of the decrease of shear strength and the change of the morphology of fracture surfaces, the thin sections of fractures treated with water cooling at different temperatures were analyzed.

Figure 10 shows some representative thin sections. At the conditions of 300 °C and one water cooling cycle, due to the

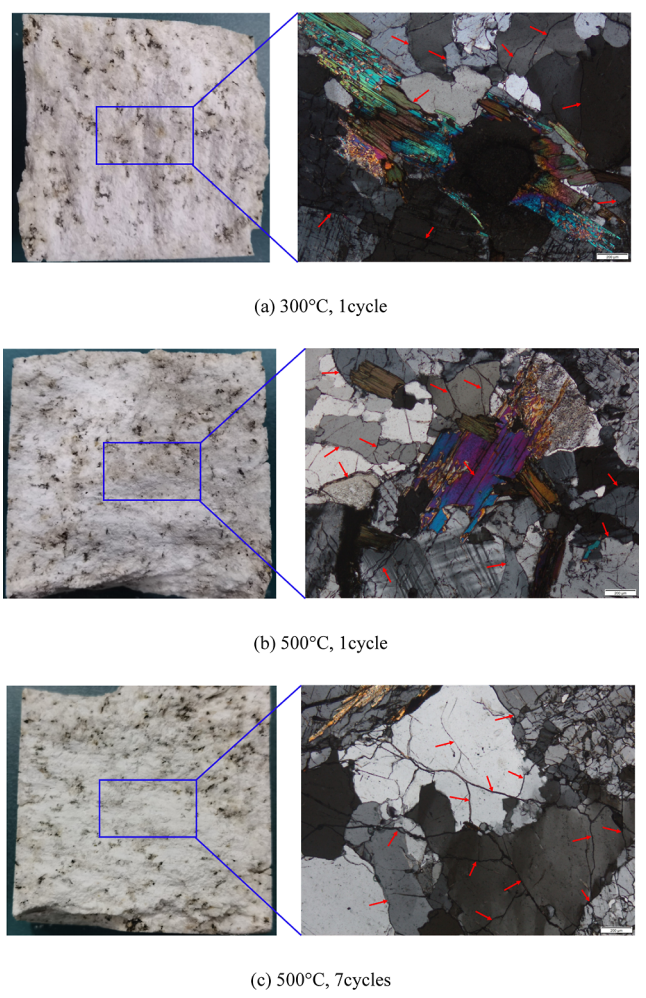

(a) 300°C, 1cycle

(b) 500°C, 1cycle

(c) 500°C, 7cycles

Figure 10. Thin section of granites.

thermal stress developed by the difference of thermal expansion between different crystals, a large number of intergranular cracks are produced between the adjacent crystal particles, and some of the crystal structures with weak strength also have intragranular fractures. When subjected to the combined action of external shear load and normal load, the input kinetic energy is transformed into elastic strain energy and stored in the microcracks. When the stored elastic strain energy is greater than the bearing limit of granites, the microcracks expand and connect with the surrounding microcracks, finally forming the macroscopic fracture surface.

Compared with the treatment condition of 300 °C, when the treatment temperature increased to 500 °C, the intragranular cracks and transgranular cracks dominated. There are two main reasons for this phenomenon: on the one hand, due to the massive loss of crystal water and structural water, the crystal skeleton is readjusted and the crystal strength is weakened,

https://doi.org/10.1021/acsomega.2c07600
ACS Omega 2023, 8, 13639−13648

which leads to the development of intragranular cracks and the occurrence of the transgranular phenomenon; on the other hand, the increased thermal stress and enhanced quenching impact further promote the development of intragranular and intergranular cracks. Under the combined action of external shear load and normal load, the connection between intragranular crack and intergranular crack is easy to occur, resulting in larger transgranular cracks. It is confirmed by previous studies that the roughness of transgranular cracks is larger than that of intragranular cracks and intergranular cracks. Therefore, the height value, apparent dip angle, and roughness of the macroscopic fracture surface increase with the increase of temperature, but the shear strength decreases.

Under the condition that the temperature remains constant at 500 °C, with the cycle times increasing to 7, the superimposed damage of thermal stress and quenching impact aggravates the propagation and interconnection between intragranular cracks and intergranular cracks, the length and width of cracks overall increase, and the transgranular phenomenon begins to become more common. The height value, apparent dip angle, and roughness of the fracture surface increase with the increase of cycle times.

4. CONCLUSIONS

In this study, the effects of temperature and cycle times on the shear behavior of intact granites and the morphological characteristics of fracture surfaces formed by shearing of intact granite were studied. The main conclusions were obtained as follows.

(1) The shear strength and shear stiffness of intact granites decrease nonlinearly with the increase of temperature or cycle times, but the height and apparent dip angle of asperities on the fracture surface increase with the increase of temperature or cycle times.

(2) The height distribution frequency of asperities on fracture surfaces treated with water cooling cycles at different temperatures can be divided into four types: right-biased peak type, left-biased peak type, left-biased middle peak, and left-biased flat peak. With the temperature and cycle times increasing, the height distribution frequency of asperities changes from right-biased peak type to left-biased flat peak, and the temperature and cycle times both increase the height and distribution uniformity of asperities.

(3) The asperity structure on the fracture surface formed by direct shearing of intact granites has asymmetric characteristics. The apparent dip angle in the reverse shear direction is larger than that in the shear direction, and the initial contact area ratio between the shear direction and reverse shear direction obtained fluctuates between 1.4 and 2.

(4) Both temperature and cycle times can change the fracturing mode of the granite crystal structure, which is also the fundamental reason why the morphology of fracture surfaces changes with temperature and cycle times.

AUTHOR INFORMATION

Corresponding Author

Tao Chen − *Great Wall Motor Co., Ltd, Baoding, Hebei 071000, China;* orcid.org/0000-0002-9942-1985; Email: 312456266@qq.com

Authors

Haiyang Jiang − *No.1 Institute of Geology and Mineral Resource Exploration of Shandong Province, Jinan 250010, China; Key Laboratory of Groundwater Resources and Environment, Ministry of Education, Jilin University, Changchun 130012, China; Shandong Engineering Laboratory for High-Grade Iron Ore Exploration and Exploitation, Jinan 250010, China*

Fengxin Kang − *College of Earth Science and Engineering, Shandong University of Science and Technology, Qingdao 266590, China; 801 Institute of Hydrogeology and Engineering Geology, Shandong Provincial Bureau of Geology and Mineral Resources (SPBGM), Jinan 250014, China; School of Water Conservancy and Environment, University of Jinan, Jinan 250022, China*

Fugang Wang − *Key Laboratory of Groundwater Resources and Environment, Ministry of Education, Jilin University, Changchun 130012, China*

Liangliang Guo − *College of Water Resources Science and Engineering, Taiyuan University of Technology, Taiyuan 030024, China*

Yanling Cao − *No.1 Institute of Geology and Mineral Resource Exploration of Shandong Province, Jinan 250010, China; Shandong Engineering Laboratory for High-Grade Iron Ore Exploration and Exploitation, Jinan 250010, China*

Complete contact information is available at: https://pubs.acs.org/10.1021/acsomega.2c07600

Notes

The authors declare no competing financial interest.

ACKNOWLEDGMENTS

This research was funded by the Shandong Provincial Natural Science Foundation (ZR2020QD122) and National Natural Science Foundation of China (grant numbers 42072331 and U1906209).

REFERENCES

(1) Bai, B.; He, Y. Y.; Li, X. C.; Li, J.; Huang, X. X.; Zhu, J. L. Experimental and analytical study of the overall heat transfer coefficient of water flowing through a single fracture in a granite core. *Appl. Therm. Eng.* **2017**, *116*, 79−90.

(2) Kang, F. C.; Li, Y. C.; Tang, C. A. Numerical study on airflow temperature field in a high-temperature tunnel with insulation layer. *Appl. Therm. Eng.* **2020**, *179*, 115654.

(3) Shakib, J. T.; Ghaderi, A.; Shahri, A. A. Analysis of hydraulic fracturing in fractured reservoir: Interaction between hydraulic fracture and natural fractures. *Science* **2012**, *9*, 393−404.

(4) Fu, P. C.; Schoenball, M.; Ajo-Franklin, J. B.; Chai, C. P.; Maceira, M.; Morris, J. P.; Wu, H.; Knox, H.; Schwering, P. C.; White, M. D.; et al. Close Observation of Hydraulic Fracturing at EGS Collab Experiment 1: Fracture Trajectory, Microseismic Interpretations, and the Role of Natural Fractures. *J. Geophys. Res.: Solid Earth* **2021**, *126*, No. e2020JB020840.

(5) Jung, H. B.; Carroll, K. C.; Kabilan, S.; Heldebrant, D. J.; Hoyt, D.; Zhong, L.; Varga, T.; Stephens, S.; Adams, L.; Bonneville, A.; et al. Stimuli-responsive/rheoreversible hydraulic fracturing fluids as a greener alternative to support geothermal and fossil energy production. *Green Chem.* **2015**, *17*, 2799−2812.

(6) Kumari, W.; Ranjith, P. G.; Perera, M.; Chen, B. K. Experimental investigation of quenching effect on mechanical, microstructural and flow characteristics of reservoir rocks: Thermal stimulation method for geothermal energy extraction. *J. Pet. Sci. Eng.* **2018**, *162*, 419−433.

(7) Shen, Y. J.; Hou, X.; Yuan, J. Q.; Xu, Z. H.; Hao, J. S.; Gu, L. J.; Liu, Z. Y. Thermal deterioration of high-temperature granite after cooling

https://doi.org/10.1021/acsomega.2c07600
ACS Omega 2023, 8, 13639−13648

shock: multiple-identification and damage mechanism. *Bull. Eng. Geol. Environ.* **2020**, *79*, 5385−5398.
(8) Kim, K.; Kemeny, J.; Nickerson, M. Effect of rapid thermal cooling on mechanical rock properties. *Rock Mech. Rock Eng.* **2014**, *47*, 2005−2019.
(9) Isaka, B. L. A.; Ranjith, P. G.; Rathnaweera, T. D.; Perera, M.; De Silva, V. Quantification of thermally-induced micro-cracks in granite using X-ray CT imaging and analysis. *Geothermics* **2019**, *81*, 152−167.
(10) Fan, L. F.; Gao, J. W.; Du, X. L.; Wu, Z. J. Spatial gradient distributions of thermal shock-induced damage to granite. *J. Rock Mech. Geotech.* **2020**, *12*, 917−926.
(11) Wu, Q. H.; Weng, L.; Zhao, Y. L.; Guo, B. H.; Luo, T. On the tensile mechanical characteristics of fine-grained granite after heating/cooling treatments with different cooling rates. *Eng. Geol.* **2019**, *253*, 94−110.
(12) Zhu, D.; Jing, H. W.; Yin, Q.; Han, G. S. Experimental study on the damage of granite by acoustic emission after cyclic heating and cooling with circulating water. *Processes* **2018**, *6*, 101.
(13) Hu, J. J.; Xie, H. P.; Sun, Q.; Li, C. B.; Liu, G. K. Changes in the thermodynamic properties of alkaline granite after cyclic quenching following high temperature action. *Int. J. Min. Sci. Technol.* **2021**, *31*, 843−852.
(14) Junique, T.; Vazquez, P.; Benavente, D.; Thomachot-Schneider, C.; Geraud, Y. Experimental investigation of the effect of quenching cycles on the physico-chemical properties of granites. *Geothermics* **2021**, *97*, 102235.
(15) Xu, C.; Sun, Q. Effects of quenching cycle on tensile strength of granite. *Geotech. Lett.* **2018**, *8*, 165−170.
(16) Gischig, V. S.; Giardini, D.; Amann, F.; Hertrich, M.; Krietsch, H.; Loew, S.; Maurer, H.; Villiger, L.; Wiemer, S.; Bethmann, F.; et al. Corrigendum to "Hydraulic stimulation and fluid circulation experiments in underground laboratories: Stepping up the scale towards engineered geothermal systems" by Gischig et al. https://doi.org/10.1016/j.gete.2019.100175. *Geomech. Energy Environ.* **2020**, *24*, 100190.
(17) Jain, C.; Vogt, C.; Clauser, C. Maximum potential for geothermal power in Germany based on engineered geothermal systems. *Geotherm. Energy* **2015**, *3*, 15.
(18) Yuan, Y. L.; Xu, T. F.; Moore, J.; Lei, H. W.; Feng, B. Coupled Thermo-Hydro-Mechanical Modeling of Hydro-Shearing Stimulation in an Enhanced Geothermal System in the Raft River Geothermal Field, USA. *Rock Mech. Rock Eng.* **2020**, *53*, 5371−5388.
(19) Khosravi, A.; Simon, R.; Rivard, P. The shape effect on the morphology of the fracture surface induced by the Brazilian test. *Int. J. Rock Mech. Min. Sci.* **2017**, *93*, 201−209.
(20) Seredin, V. V.; Leibovich, L. O.; Pushkareva, M. V.; Kopylov, I. S.; Khrulev, A. S. Evolution of fracture surface morphology in rocks. *J. Min. Sci.* **2013**, *49*, 409−412.
(21) Liu, Y.; Huang, D.; Cen, D.; Zhong, Z.; Gong, F. Q.; Wu, Z. J.; Yang, Y. T. Tensile Strength and Fracture Surface Morphology of Granite Under Confined Direct Tension Test. *Rock Mech. Rock Eng.* **2021**, *54*, 4755−4769.
(22) Chen, Y.; Cao, P.; Mao, D. W.; Pu, C. Z.; Fan, X. Morphological analysis of sheared rock with water-rock interaction effect. *Int. J. Rock Mech. Min. Sci.* **2014**, *70*, 264−272.
(23) Yang, X. X.; Sun, D. K.; Jing, H. W. Morphological features of shear-formed fractures developed in a rock bridge. *Eng. Geol.* **2021**, *278*, 105833.
(24) International Society for Rock Mechanics and Rock Engineering. *The Complete ISRM Suggested Methods for Rock Characterization, Testing and Monitoring*; International Society for Rock Mechanics and Rock Engineering: Salzburg, Austria, 2007.
(25) Genter, A.; Evans, K.; Cuenot, N.; Fritsch, D.; Sanjuan, B. Contribution of the exploration of deep crystalline fractured reservoir of Soultz to the knowledge of enhanced geothermal systems (EGS). *C. R. Geosci.* **2010**, *342*, 502−516.
(26) Gischig, V.; Giardini, D.; Amann, F. Hydraulic stimulation and fluid circulation experiments in underground laboratories: Stepping up the scale towards engineered geothermal systems. *Geomech. Energy Environ.* **2019**, *24*, 100175.
(27) Ohno, I. Temperature Variation of Elastic Properties of .ALPHA.-Quartz up to the .ALPHA.-.BETA. Transition. *J. Phys. Earth* **1995**, *43*, 157−169.
(28) Chen, S.; Yang, C.; Wang, G. Evolution of thermal damage and permeability of Beishan granite. *Appl. Therm. Eng.* **2017**, *110*, 1533−1542.
(29) Xia, C. C.; Tang, Z. C.; Xiao, W. M.; Song, Y. L. New peak shear strength criterion of rock joints based on quantified surface description. *Rock Mech. Rock Eng.* **2014**, *47*, 387−400.
(30) Yang, J.; Rong, G.; Hou, D.; Peng, J.; Zhou, C. Experimental study on peak shear strength criterion for rock joints. *Rock Mech. Rock Eng.* **2016**, *49*, 821−835.
(31) Grasselli, G.; Wirth, J.; Egger, P. Quantitative three-dimensional description of a rough surface and parameter evolution with shearing. *Int. J. Rock Mech. Min. Sci.* **2002**, *39*, 789−800.
(32) Tatone, B. S. A.; Grasselli, G. A method to evaluate the three-dimensional roughness of fracture surfaces in brittle geomaterials. *Rev. Sci. Instrum.* **2009**, *80*, 125110.
(33) Liu, Q. S.; Tian, Y. C.; Liu, D. F.; Jiang, Y. L. Updates to JRC-JCS model for estimating the peak shear strength of rock joints based on quantified surface description. *Eng. Geol.* **2017**, *228*, 282−300.
(34) Chen, B.; Shen, B.; Jiang, H. Shear mechanical behavior of intact granite under mechanical-thermal coupling and 3D morphology of shear-formed fractures. *Journal of Rock Mechanics and Geotechnical Engineering* **2023**, *15*, 523−537.
(35) Chen, B.; Shen, B.; Zhang, S.; Li, Y.; Jiang, H. 3D morphology and formation mechanism of fractures developed by true triaxial stress. *International Journal of Mining Science and Technology* **2022**, *32*, 1273−1284.

https://doi.org/10.1021/acsomega.2c07600
ACS Omega 2023, 8, 13639−13648